

# Adaptive Real-Time Decomposition of Electromyogram During Sustained Muscle Activation: A Simulation Study

Yang Zheng Dand Xiaogang Hu D

Abstract-Objective: Real-time decomposition of electromyogram (EMG) into constituent motor unit (MU) activity has shown promising applications in neurophysiology and human-machine interactions. Existing decomposition methods could not accommodate stochastic variations in EMG signals such as drifts of action potential amplitudes and MU recruitment-derecruitment (rotation) patterns during long-term recordings. The objective of this study was to develop an adaptive real-time decomposition approach suitable for prolonged muscle activation. *Methods*: We developed a parallel-double-thread computation algorithm. The backend thread initiated and periodically refined and updated the MU information (separation matrix) using independent component analysis and convolution kernel compensation. The frontend thread performed the real-time decomposition. We evaluated our algorithm on synthesized high-density EMG signals, in which MUs were recruitedderecruited sporadically and MU action potentials amplitude drifted over time. Different signal-to-noise levels were also simulated. Results: Compared with the decomposition without the adaptive processes, periodically fine-tuned and updated separation matrix increased identifiable MU number by 3-4 fold over 30-minute of signals. The increased MU number was more prominent at higher signal-to-noise ratios. The decomposition accuracy also increased by up to 10% with greater improvement observed at higher muscle contraction levels. Conclusion: The adaptive algorithm can maintain the decomposition performance over time, allows us to continuously track the same MUs during sustained activation, and, at the same time, can add newly recruited MU information to existing separation matrix. Significance: Our approach showed robust performance over time, which has the potential to longitudinally evaluate MU firing and recruitment properties and improve neural decoding performance for neural-machine interactions.

Manuscript received March 18, 2021; revised June 6, 2021; accepted August 3, 2021. Date of publication August 6, 2021; date of current version January 20, 2022. This work was supported in part by the National Science Foundation under Grants CBET-1847319 and IIS-2106747. (Corresponding author: Xiaogang Hu.)

Yang Zheng is with the Institute of Engineering and Medicine Interdisciplinary Studies, School of Mechanical Engineering, Xi'an Jiaotong University, China.

Xiaogang Hu is with the Joint Department of Biomedical Engineering, University of North Carolina-Chapel Hill and NC State University, Chapel Hill, NC 27599 USA (e-mail: xiaogang@unc.edu).

This article has supplementary downloadable material available at https://doi.org/10.1109/TBME.2021.3102947, provided by the authors. Digital Object Identifier 10.1109/TBME.2021.3102947

Index Terms—Source separation, independent component analysis, adaptive decomposition, online signal processing.

#### I. INTRODUCTION

S AN basis of muscle activation, motor units (MUs) transform motoneuron firing activities into contractions of muscle fibers [1]. The forces generated by a muscle largely depend on the number and the firing rate of active MUs [2], [3]. Understanding MU activity can provide insight into the physiological and pathological conditions of the neuromuscular system [4]–[6]. In neural rehabilitation, population level MU firing frequency has also been utilized to interface with assistive devices [7], [8], because the compound firing rate of a number of MUs reflects the neural drive to the muscles [7], which has been used to estimate fingertip forces [9], [10] or finger kinematics [11], [12]. Historically, individual MU activities are captured through intramuscular electrodes [13], and are extracted using semi-automatic decomposition algorithms [14], [15]. Because of the small recording volume, however, intramuscular recordings can only obtain a limited number of MUs, limiting the ability to capture populational neural activities.

Alternatively, recent development of multi-channel surface electromyogram (sEMG) electrodes paired with source separation algorithms can separate a large number of MUs (firing and recruitment patterns) from multi-channel sEMG signals noninvasively. For example, using an unique 4-channel surface electrode array, an automatic decomposition method has been developed based on template-matching of MU action potentials (MUAPs) [16]. More recently, with the development of high-density EMG (HD EMG) electrode grid, blind source separation techniques have been utilized to decompose HD EMG signals. For instance, the convolution kernel compensation (CKC) [17] and different independent component analyses (ICA) algorithms [18]–[23] have been used to extract MU firing activities.

Although widely used in research, these source separation algorithms are computationally intensive, and the EMG signals need to be processed offline. To enable real-time decomposition for neural-machine interface applications, earlier studies have used sequential two-step calculation approaches to obtain MU activities in real-time [7], [8], [24], [25]. Typically, the first initialization step calculates the MU information (separation matrix or MUAP shape features) offline using an initial segment of

0018-9294 © 2021 IEEE. Personal use is permitted, but republication/redistribution requires IEEE permission. See https://www.ieee.org/publications/rights/index.html for more information.

EMG signals, and the second step then applies the pre-calculated MU information to newly acquired EMG signals in real-time, assuming that the separation matrix or MUAP shape features are preserved in subsequent EMG segments.

However, the sequential two-step approaches have several limitations when MU information is calculated only in the initialization step. First, the quality of the initial MU information, hence the performance of the subsequent real-time decomposition, are heavily determined by the signal quality of the initial data segment. A high signal quality is not guaranteed in certain situations. Second, the initial calculation step cannot capture newly recruited MUs, especially during sustained muscle contractions. MU rotation, a sporadic recruitment-derecruitment pattern alternating between MUs, commonly occurs during prolonged muscle contractions [26]–[28]. Finally, the validity of the initial MU information can degrade over time due to variations of the EMG signals, which can arise from changes in noise level or MUAP amplitude drift due to a shift of the recording electrodes relative to the muscles.

To address these limitations, we developed a parallel-doublethread computation algorithm that can accommodate periodic and stochastic variations in HD EMG signals during prolonged muscle contractions. The backend thread first initiated and then periodically refined and updated the separation matrix using FastICA and CKC algorithms. The novelty of the backend thread is twofold. First, the refinement of separation vectors of previously identified MUs maintained their validity amid EMG signal variations, thereby accurately tracking the same MUs over sustained muscle contractions. Second, the update of separation matrix (extending the dimension of the matrix) allowed the identification of newly recruited MUs or previous active MUs that were not identifiable during initialization. The frontend thread applied the most current separation matrix to new EMG segments to extract MU activities in a real-time manner. We evaluated the parallel-double-thread algorithm using simulated HD EMG signals, since the ground-truth of MU firing and recruitment activities are known. The MUs were alternately recruited and derecruited in a stochastic manner using a MU rotation model. MUAP amplitude of different MUs drifted over time, and different background noise levels of the simulated EMG were also simulated. The results showed an increased number of identified MUs and an improved decomposition accuracy. Our approach revealed robust performance over prolonged muscle contractions. The algorithm allowed longitudinal tracking of MU firing and recruitment properties, in order to address mechanistic research questions or to perform clinical assessments. The outcomes could also lead to robust performance of neural decoding for neural-machine interactions during long-term recordings.

### II. METHODS

# A. Simulated EMG Signals With MU Rotation

To synthesize EMG signals, we used a previously developed MU pool model [29] to first generate firing activities of individual MUs under a pseudorandom neural drive trajectory. We then developed a MU rotation model such that rotation occurred

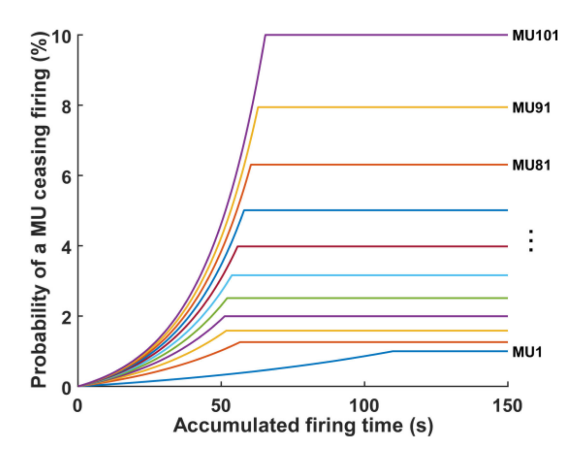


Fig. 1. Accumulated firing time versus probability of ceasing firing under the RL condition. The probabilities for every 10th MU in the pool are shown.

randomly between MUs. Finally, we used a convolution model to generate the HD EMG signals.

1) MU Pool Model: The MU pool model mainly included the recruitment and rate coding of individual MUs [29]. Briefly, the recruitment thresholds of MUs varied such that most of the MUs were recruited at a low neural drive. The number of recruited MUs was determined by the excitation neural drive to the MU pool. The shape of the neural drive signal used here was a series of trapezoids with their plateau levels varying pseudo-randomly between 10% MVC and 45% MVC. Under this neural drive profile, 80 MUs were recruited in total. The mean firing rate of MUs increased linearly with the neural drive signal before reaching their peak firing rates [29]. The peak firing rate of MUs was higher with a lower threshold. To simulate the stochastic nature of the MU firings, the instantaneous firing rate varied with a coefficient of variation of 0.2.

2) MU Rotation Model: The MU rotation model had the following key features. First, rotation occurred randomly. For an active MU, the probability of ceasing firing increased with the accumulated firing time (i.e., time since recruitment). Second, the ceasing firing probability of the fatigue-resistant low-threshold MUs was lower than that of the fast-fatigable high-threshold MUs. Third, rotation occurred between MUs with similar recruitment thresholds.

Based on the first two features, the probability of ceasing firing for individual MUs was determined by:

$$P(i) = \min(B(e^{i^A \cdot R \cdot t} - 1), \quad P_1 \cdot e^{a(i-1)})$$

$$a = \ln(P_n/P_1)/(n-1)$$

$$i = 1, 2, \dots, n, \quad t > 0$$
(1)

where *i*represents the *i*th MU and indicates the recruitment order of MUs, n is the total number of MUs in the model, t is the accumulated firing time, which was calculated relative to the time of recruitment of individual MUs. The probability of ceasing firing increased exponentially with time until it reached the maximum (Fig. 1). Awas the MU factor which determined the probability difference between MUs and was set to 1/3 in this

study. B was the amplitude factor that scaled the amplitude of the probability of ceasing firing for a specific MU at a specific time, and was set to 1/200. R was the time factor which determined the increase rate of the probability with time. The maximum probability of ceasing firing for individual MUs also increased exponentially with the index number of MUs.  $P_1$  and  $P_n$  were the maximum probability of the first and the nth MUs, respectively. More details on the influence of individual parameters on the probability of ceasing firing are included in Supplementary Material Section A.

In this study, two combinations of the three constants  $(R, P_1, P_n)$  were used to simulate two different levels of MU rotation. At the high rotation (RH) level,  $R, P_1$ , and  $P_n$  were set to 0.02, 0.05, and 0.2, respectively. At the low rotation (RL) level,  $R, P_1$ , and  $P_n$  were set to 0.01, 0.01, and 0.1, respectively. Compared with the RL condition, the rotation occurred more frequently under the RH condition.

To simulate MU rotation, the spike trains obtained in the MU pool model were modified by assigning the active or inactive status to each of the individual MUs. For a given MU, the spikes within the inactive time window were eliminated. For simplicity, we prescribed the rotation occurrence within a rotation group of 2 or 3 MUs, and only one MU discharged at any time. In addition, a MU can only be selected in one rotation group. If a rotation happened, the active MU ceased firing and the other MU in the rotation group started firing (more details in Supplementary Material B). The MU rotation procedure was repeated in individual trials so that the rotation situation differed between trials.

3) Convolution Model: The HD EMG signals can be synthesized using a convolutive mixture [14], [22] between a series of delta functions (which represented the discharge timings of MUs) and the corresponding impulse responses (which represented the motor unit action potentials (MUAP)) (more details in Supplementary Material C). The MUAP template pool for individual MUs was obtained from previous experimental HD EMG data using an  $8 \times 8$  square electrode grid [30], through a spike triggered average of the EMG signals [31]. Each simulated MU had  $8 \times 8$  MUAP templates, and the templates were randomly assigned to individual MUs between trials. The MUAP amplitude varied or scaled randomly for each spike following a uniform distribution U(0.9, 1.1), in order to simulate the spike-by-spike variations in the MUAP amplitude during experiment recordings. The random variation of MUAP amplitude can arise from change of electrode-skin contact resistance and small displacement between muscle fibers and electrodes during muscle contractions. In addition, the amplitude also had a time-dependent drift (either increased or decreased) by k% over the duration of the trial, considering the sustained contractions of the muscle fibers. Two levels of amplitude drift were tested:  $k \in U(20, 40)$  for the high amplitude (AH) drift and  $k \in U(2, 10)$  for the low amplitude (AL) drift.

Lastly, baseline noise was added to the EMG signals. Two different levels: signal-to-noise ratio (SNR) at 5 dB and 10 dB were simulated. The SNR was defined as the logarithmic ratio between the variance of the clean EMG signals and the variance of white Gaussian noise added to the clean EMG. To this end,

there were 8 conditions: two MU rotation level (RH and RL), two amplitude drift level (AH and AL) and two baseline noise levels (SNR5 and SNR10). In each condition, 10 trials were simulated, and each trial lasted for 30 minutes. The sampling rate was 1024 Hz.

## B. Basis of Decomposition Algorithm

1) FastICA-Based Separation Vector Extraction: The FastICA-based EMG decomposition method was used to extract the information of MUs. The original EMG signals were first extended and whitened, resulting in the EMG matrix . Then, the FastICA algorithm was performed multiple iterations on and each iteration output the information of one MU including the source signal s, the spike train t, and the separation vector w. The source signal was calculated by multiplying the extended and whitened EMG data by the separation vector

$$\mathbf{s} = \mathbf{w}^{\mathrm{T}} \underline{\mathbf{z}} \tag{2}$$

The spike train was obtained via a binary classification of the peaks in the source signal using the *Kmeans*++ algorithm [32]. The separation vectors that corresponded to motion artifacts, with poor quality, or were duplicates of other MUs were removed. More details can be found in previous studies [33], [34]. The separation vectors of all retained MUs constituted the separation matrix, which can be applied to new EMG data to extract spike trains in real-time.

2) CKC-Based Separation Vector Refinement: With prolonged muscle contractions, the separation vectors from the FastICA algorithm may become suboptimal due to the rotation of MUs and drifts of the MUAP amplitude, resulting in inaccurate spike detection. Therefore, the separation vectors of previously identified MUs were refined during an separation matrix updating procedure via the CKC algorithm [17] using new EMG data (termed CKC-based iteration in the subsequent text, see Supplementary Material D). The CKC-based iteration has been used to refine separation vectors previously [23].

3) MUAP Similarity Index: During separation vector refinement, the newly obtained separation vector must correspond to the same MU of the previously extracted separation vector. We compared the similarity of the MUAP corresponding to the two separation vectors obtained at different times to verify that they belonged to the same MU. Given two MUs with their MUAPs denoted as  $x_i(t)$  and  $y_i(t)$ ,  $i = 1, 2, \ldots, m, t = 1, \ldots, T$ , the similarity of the two MUAP was defined as (termed MUAP similarity index):

$$SI = 1 - \frac{\sum_{i} D_{i} W_{i}^{c-1}}{\sum_{i} W_{i}^{c}}$$
 (3)

with 
$$D_i = \sum_t (x_i(t) - y_i(t))^2$$
 and  $W_i = \sum_t (|x_i(t)| + |y_i(t)|)^2$ . It can be regarded as the weighted average of the MUAP

It can be regarded as the weighted average of the MUAP difference across m channels, and it ranged from 0 to 1. The constant c was a scaling factor to adjust the weight distribution between channels with different energy levels. In our preliminary study, we calculated the MUAP similarity indices of MUs in the MU pool used to simulate the EMG signals, and c was set to 4 in this study because it can distinguish different simulated

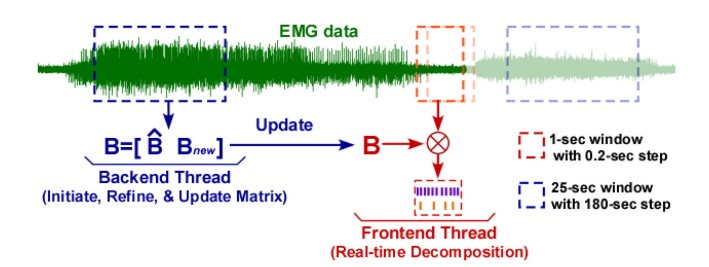


Fig. 2. An illustration of the parallel-double-thread approach. The backend thread initiates, refines, and updates the separation matrix using a 25-second window every 3 minutes.  $\hat{B}$  contains separation vectors of previously identified MUs with some of them refined.  $B_{new}$  contains separation vectors of newly identified MUs. The real-time frontend thread extracts MU spikes using a 1-second sliding window with a 0.2-second step.  $\otimes$ : apply the separation vectors to EMG signals after extension and whitening.

MUs appropriately. If the MUAP similarity index was larger than a threshold (i.e., 0.95), the two MUs were considered as the same MU.

# C. Adaptive Real-Time Decomposition Algorithm

The separation matrix calculation procedures including the FastICA and CKC iterations were time-consuming and cannot be performed in real-time. Because MU rotation does not occur frequently, and the amplitude of MUAP is generally stable within a short time frame, it is possible to update the separation matrix and extract the MU firing events in two parallel threads (Fig. 2). In the backend thread, the initiation, refinement, and update of separation matrix were performed at intervals of 3 minutes, and the original matrix then was replaced with the updated separation matrix in the frontend thread. In the frontend decomposition thread, firing events of individual MUs were extracted in real-time by applying the separation vectors to EMG data.

1) Initialization Phase: For each 30-minute trial, the first 25-second segment was used to initialize the separation matrix with 80 FastICA iterations. The separation vectors corresponding to motion artifacts, poor source signal quality, and duplicates of other MUs were removed. The separation matrix Bconsisted of all the retained separation vectors.

After the initialization, the refinement and update of the separation matrix, using CKC and FastICA, were performed every 3 minutes using the 25-second window (Fig. 2). The updating interval of 3 min was selected based on an earlier work that showed stable decomposition performance till approximately 200-240 s of activation [25].

- 2) Matrix Refinement via CKC-Based Iteration: The CKC-based refinement procedure was first performed for individual separation vectors. We utilized the MUAP similarity index to determine the consistency of the MUs before and after the refinement, such that the separation vector was updated only if the refined separation vector corresponded to the same MU as the original one (more details in Supplementary Material E).
- *3) Matrix Update via FastICA:* After the refinement procedure, the FastICA algorithm was performed on the 25-second EMG segment with 50 iterations. In addition, to accurately

extract MUAPs of newly identified MUs, only the MUs that had more than 100 spikes were retained. These retained MUs can either be previously identified or newly identified. A two-step method was used to determine whether a newly identified MU was a duplicate of a previously identified MU, by assessing both the synchronization level of the spike trains and the similarity of the MUAP waveforms. If both the synchronization level (80%) and the similarity (0.95) exceeded a given threshold, the MU was considered a duplicate MU. More details can be found in Supplementary Material F. Therefore, the separation vectors of the previously identified MUs can be updated using the new separation vectors. In some cases, multiple MUs could be duplicates of the same MU, and only the one with the highest source signal quality was used to replace the previously identified MU.

To this end, the separation matrix  $\hat{B}$  contained the separation vectors of all previously identified MUs. Some of the separation vectors were refined using CKC or replaced by the separation vectors from FastICA. The new MUs were pooled together and constituted the separation matrix  $B_{new}$ . The separation matrix was updated as  $B = [\hat{B} \ B_{new}]$  (Fig. 2).

#### D. Performance Evaluation

The performance evaluation mainly focused on two aspects: the number of identified MUs and the accuracy of the spike detection. These two outcome measures were evaluated with and without the matrix refinement and update procedures (termed update vs. no update in subsequent text for simplicity). The number of identified MUs was calculated every time after the separation matrix was updated. The percentage of MU number was calculated by normalizing the number of all recruited MUs for the entire 30-min trial, i.e., 80 MUs. The accuracy of spikes from the MUs identified in the initialization phase was compared between the two methods, given that the method without matrix update could not identify new MUs. Specifically, the accuracy calculation involved two steps. We first identified the simulated MUs (ground-truth) corresponding to individual spike trains decomposed in the offline initialization phase (25 seconds). The ground-truth were the spike trains used to simulate the EMG signals. To accomplish that, we calculated the consistency between the spike train of a given decomposed MU in the initialization phase and all the MU spike trains used to simulate the EMG. The spike train with the highest consistency was considered corresponding to the given simulated MU. The consistency between two spike trains was calculated as:

$$C = \frac{2M_{com}}{M_1 + M_2} \times 100\% \tag{4}$$

where  $M_1$  and  $M_2$  are the number of spikes in two spike trains respectively and  $M_{com}$  is the number of spikes that are synchronized between two spike trains. This procedure was repeated for all decomposed MUs, and their corresponding true spike trains were obtained. Second, we calculated the weighted average of the consistency between MU spike trains obtained via the online decomposition and their corresponding true spike trains using a 1-minute window with no overlap. The overall decomposition

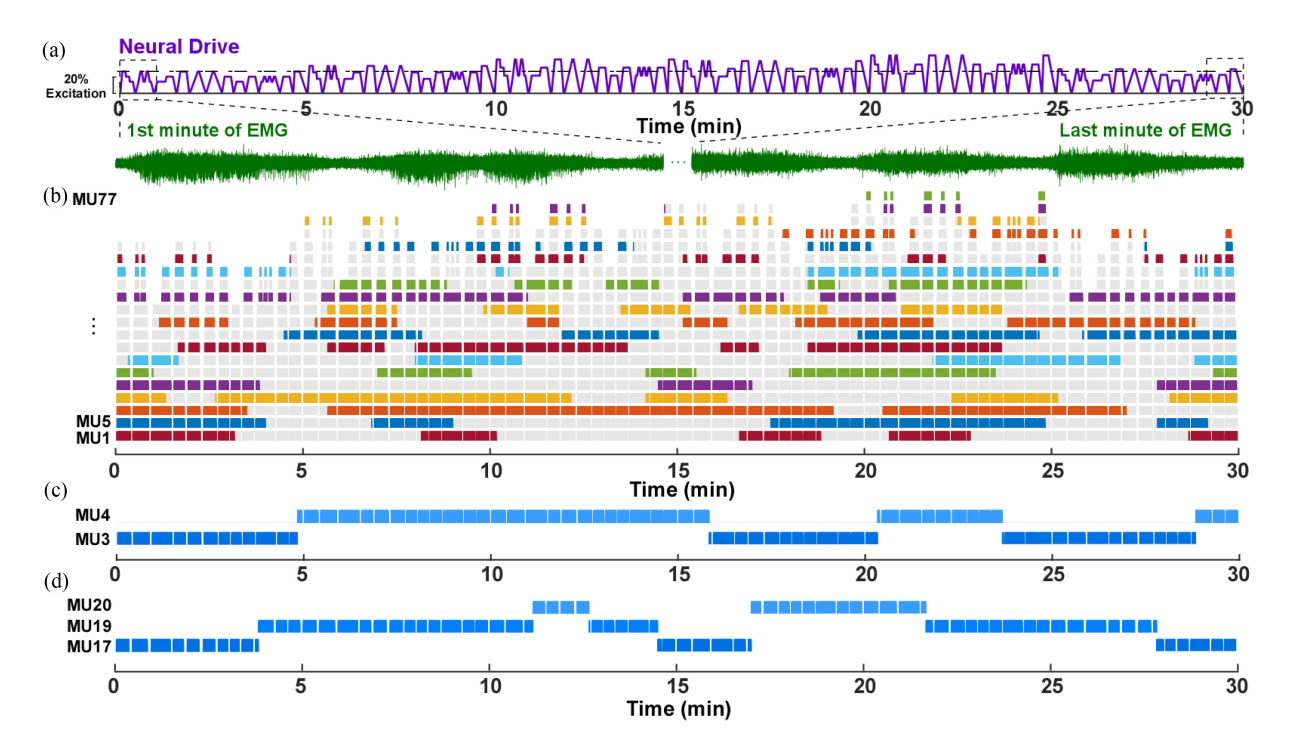


Fig. 3. The simulated neural drive ranging from 0-45% maximum excitatory drive (y-axis), and a representative single channel EMG of the first and last 1-minute of signals (A). The spike trains used to simulate the EMG signals of a representative trial (B). The spike trains of every 5 MUs are illustrated. The spikes with gray color are eliminated in the MU rotation procedure. Rotation occurs between two MUs (C) and between three MUs (D) from the same trial as examples.

accuracy was calculated as the weighted average of the consistency across *N* number of MUs:

$$C_{ave} = \sum_{i=1}^{N} d_i C_i$$

$$d_i = \frac{M_i^{\text{det}} + M_i^{true}}{\sum_{i=1}^{N} (M_i^{\text{det}} + M_i^{true})}$$
(5)

where  $C_i$  is the consistency of the *i*th MU calculated using Equation (4) between the decomposed spike train and its corresponding true spike train, and  $d_i$  is the weight of the *i*th MU.  $M_i^{\text{det}}$  is the number of decomposed spikes of the *i*th MU and  $M_i^{\text{true}}$  is the number of true spikes of the *i*th MU. Instead of calculating the arithmetic average, we calculated the weighted average to balance the influence of MUs with different number of spikes on the consistency values across all MUs. For example, when a MU only had one firing spike in a time window and it was not successfully identified, the consistency of the MU was 0%. Due to its small weight, its consistency would not significantly influence the weighted average consistency across all MUs.

#### III. RESULTS

# A. MU Rotation

Fig. 3A illustrates the simulated neural drive ranging from 0-45% maximum excitatory input and a representative single channel EMG of the first and last 1-minute. Fig. 3B illustrates the spike trains used to simulate the EMG signals of a representative

trial. MU rotation occurred randomly between MUs with similar recruitment thresholds such as between MUs 3 and 4, and between MUs 17, 19, and 20 (Fig. 3C and 3D). In addition, the duration of continuous firing of lower threshold MUs (e.g., MUs 3 and 4) was generally longer compared with higher threshold MUs (e.g., MUs 17, 19, and 20). The compound firing rate of all MUs should reflect the neural drive signal to the MU pool. To verify whether it was still true with MU rotation, the correlation coefficient between the neural drive signal and the compound firing rate was calculated for individual trials. The average correlation coefficient was  $0.9810\pm0.0015$  across all the 40 trials in the RH condition and  $0.9819\pm0.0018$  across all the 40 trials in the RL condition.

## B. Identified MU Number

One major goal of updating the separation matrix was to identify more MUs. Fig. 4A illustrates the number of identified MUs over time in different simulated conditions. For all the conditions, only approximate 13% MUs can be identified during the initialization phase. With separation matrix update every 3 minutes, the number of identified MUs increased initially and then plateaued at a level where approximate 45% MUs can be identified. The numbers of identified MUs of the 1st minute and the  $28^{th}$  minute were compared between the decomposition methods with and without matrix updates. The two-way ANOVA showed that the *Method* had a significant influence on the MU number (F(1,9) = 4446.74, p < 0.001) across all conditions. Namely, matrix update significantly increased the number of

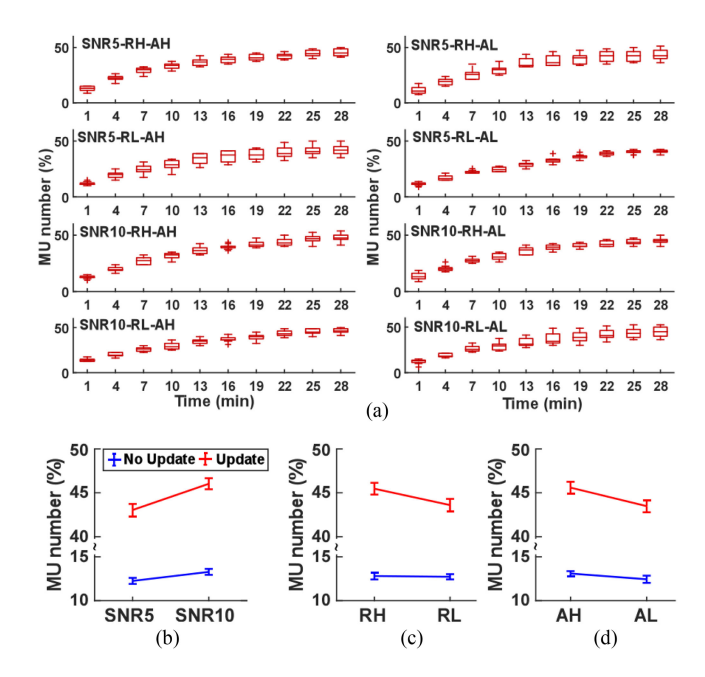


Fig. 4. Box-plots of the % number of identified active MUs across all 10 trials over time for individual conditions when the separation matrix was updated every 3 minutes (A). The number of MUs without update did not change and was equal to the number of MUs of the initialization phase. The MU number was normalized by the number of all recruited MUs in the entire trial which was consistent across trials and conditions. MU number with trials that had the same SNR level (B), rotation level (RH vs. RL) (C), and MUAP amplitude drift level (AH vs. AL) (D) grouped together, respectively. The error bars represent the standard error.

identified MUs. We also observed a significant interaction between *Method* and *SNR level* (F(1,9) = 4.087, p = 0.047) as shown in Fig. 4B. However, there was no significant interaction between *Method* and *Rotation level* (F(1,9) = 3.574, p = 0.063), nor between *Method* and *MUAP amplitude drift* (F(1,9) = 2.241, p = 0.139) as shown in Figs. 4C and 4D.

The time needed to extract the spikes of individual MUs for each 1-second window should be less than 0.2 seconds to satisfy real-time processing. As expected, the results showed that the calculation time for each 1-second window depended on the identified MU number. It first increased and then plateaued, and the calculation time at the end of the trials was approximately 0.06 seconds (Supplementary Material G), which was consistent across trials. For some data segments, the calculation time was longer compared with adjacent segments. However, the calculation time was well below 0.1 seconds.

# C. Spike Detection Accuracy

MU rotation and MUAP amplitude drift can influence the accuracy of the decomposition. The separation matrix update method could maintain decomposition performance despite of these interferences. Fig. 5 shows the true spike train and the spike trains obtained with and without separation matrix updates. The results of the initial 11.5-minute segment from a representative MU are illustrated in Fig.s 5A and 5B. Both methods had high accuracy within the first 8 minutes. Beyond that, the accuracy of the method without matrix update decreased gradually. With

matrix update, the accuracy also decreased and was comparable with the other method between the 8<sup>th</sup> and 9<sup>th</sup> minute. However, when the separation matrix was updated after the 9<sup>th</sup> minute, the accuracy was consistently higher. Figs.5C and 5D illustrate the results of a different MU. Both methods had poor accuracy before the 21<sup>st</sup> minute. Without matrix update, the initial separation vector failed to detect spikes of the MU. On the contrary, with matrix update between 21<sup>st</sup> and 22<sup>nd</sup> minute, the accuracy increased to 50%. The second update of the matrix between 24<sup>th</sup> and 25<sup>th</sup> minute further increased the accuracy to above 90%. These representative results indicated that the matrix update method could improve the decomposition accuracy over time.

Fig. 6 illustrates the average accuracy over time across 10 trials for individual conditions. In general, the accuracy decreased from the initial high level and fluctuated throughout the trials. The accuracy was relatively low between 20-25 seconds due to high neural drive as shown in Fig. 3A. In most cases, the accuracy obtained with matrix update was higher than without matrix update. Furthermore, both methods showed higher accuracy at the SNR10 condition than the SNR5 condition. The degree of improvement with matrix update was smaller at the RH level compared with the RL level. To further quantify the influence of different factors on decomposition accuracy, the accuracy was averaged across time for individual trials (Fig. 7). The ANOVA showed that the Method had a significant influence on the accuracy (F(1,9) = 98.39, p < 0.001). We also found a significant interaction between *Method* and the *Rotation level* (F(1,9) = 7.173, p = 0.009) as shown in Fig. 7C. However, there was no significant interaction between Method and SNR level (F(1,9) = 3.167, p = 0.079), nor between *Method* and *MUAP* amplitude drift (F(1,9) = 0.002, p = 0.961) as shown in Figs.7B and 7D. Further pairwise comparison with Holm-Bonferroni correction showed that updating the separation matrix improved the accuracy in 7 conditions (p < 0.05). However, in the SNR10-RH-AH condition, the improvement was not significant (p > 0.05).

## IV. DISCUSSION

The objective of this study was to develop an adaptive real-time MU decomposition algorithm. We implemented a parallel-double-thread computation algorithm, with the frontend thread performing real-time decomposition and the backend thread performing separation matrix updates at fixed intervals. The separation matrix updates were designed to alleviate performance degradation of MU decomposition caused by MU rotation (sporadic recruitment-derecruitment) and MUAP amplitude drift during prolonged muscle contractions. The novel backend algorithm can periodically update separation vectors of previously identified MUs, which can maintain their validity amid EMG variations and allow the possibility to continuously track the same MUs during sustained activation. The update of separation matrix can also extend the dimension of the matrix, which allowed the identification of newly recruited MUs or active MUs that were not identified during initialization. Because the ground-truth of MU firing activities from experimental EMG

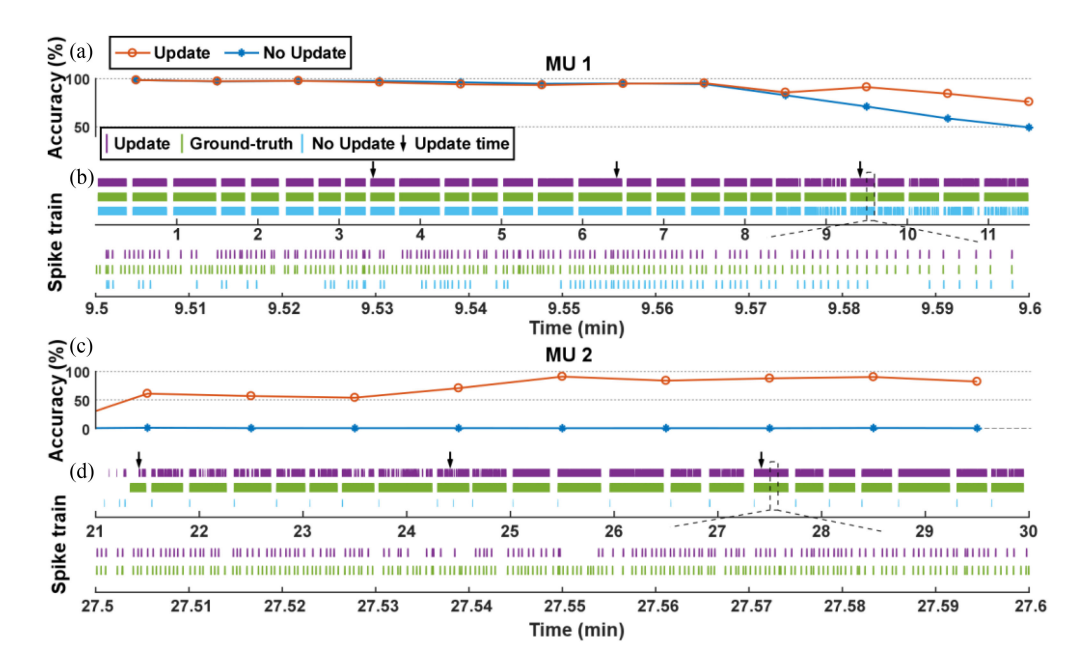


Fig. 5. A comparison between the true spike train and the spike trains obtained through the two methods from two representative segments of MU 1 (A, B) and MU 2 (C, D). Two 0.1-minute segments of spike trains are shown in B and D, respectively, to illustrate more detailed spike timings.

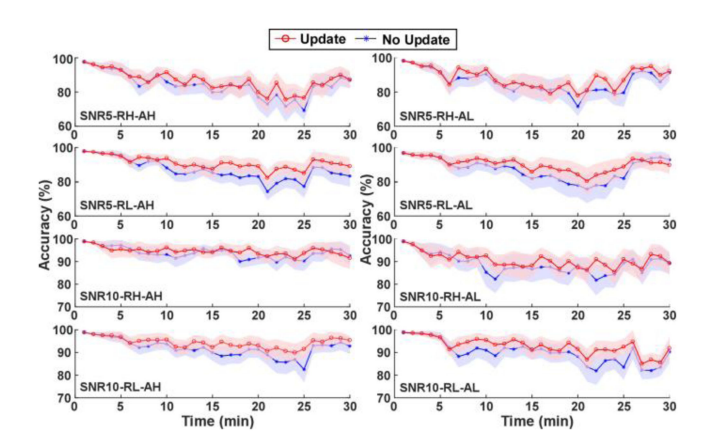


Fig. 6. The overall decomposition accuracy over time across 10 trials for individual conditions. The shaded region represents the standard error of accuracy across MUs in each trial at a given time.

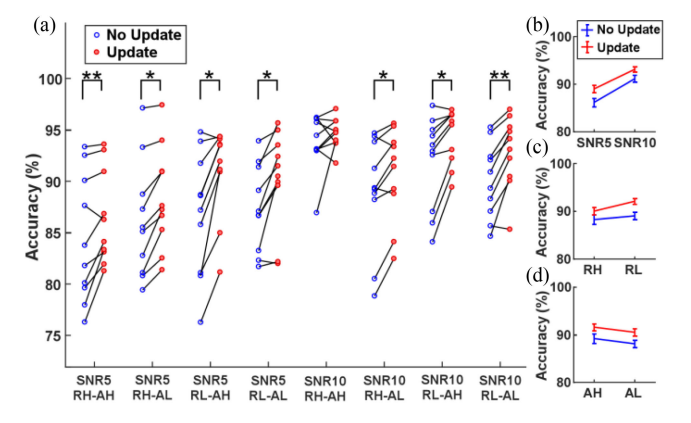


Fig. 7. Spike detection accuracy averaged across time for individual trials in individual conditions (A). Average accuracy in trials with the same SNR level (B), rotation level (C), and MUAP amplitude drift level (D), respectively. The error bars represent the standard error. \*, p < 0.05. \*\*, p < 0.01.

recordings is typically unknown, we utilized synthesized EMG signals to evaluate the performance of our method. Compared with conventional real-time decomposition, the results showed that our adaptive decomposition method can identify a larger number of MUs over time, including some newly recruited MUs. In addition, updating the separation vectors of MUs identified earlier improved the decomposition accuracy, compared with the conventional method where the separation vectors were fixed over time. These results demonstrated the robust performance of the adaptive approach, which has the potential to improve the performance of neural decoding for applications such as myoelectric continuous control of assistive devices.

To mimic sporadic MU de-recruitment and recruitment during prolonged muscle contractions, we developed a stochastic MU rotation model. The MU rotation model can reflect the physiological regulation of MU activities qualitatively [26]–[28]. The

rotation can occur randomly with the probability determined by the accumulated firing time and the recruitment thresholds of MUs. However, the selection of the absolute value of the probability was arbitrary, mainly due to a lack of systematic investigation from experimental studies. Nonetheless, the general stochastic MU rotation behavior was simulated, and the compound firing rate with MU rotation had a high correlation with the neural drive signal to the MU pool. This was mainly because the rotation was prescribed to occur between MUs with similar recruitment thresholds, and the firing rate properties of these MUs were also similar. This MU rotation model allows us to evaluate the performance of our separation matrix update method, and has the potential to be utilized in other scenarios where periodic MU recruitment-derecruitment activity needs to be considered.

In all the simulated conditions, the number of identified MUs increased significantly when the separation matrix was updated. Specifically, the initialization phase can only identify approximately 13% of the total MUs. With updated separation matrix over time, however, almost 50% of the total MUs can be identified at the end of the trial. With successive matrix update, the number of MUs first increased and then plateaued. The plateau can arise from the fact that the algorithm could not identify all the MUs in the current matrix update configuration, such as the current number of FastICA iterations. These results demonstrated the potential of our method to identify newly recruited MUs when MU rotation occurs. This is critical because the inability to identify newly recruited MUs could lead to decomposition performance degradation over prolonged muscle contractions. For example, the muscle contraction level could be underestimated, when some of the initially identified MUs cease firing and the newly recruited MUs are not identified. This could partly explain the increase of the force estimation error over time without updating the MU pool [25].

With matrix update, the separation vectors of some previously identified MUs could be fine-tuned to improve the accuracy as shown in Fig. 7. The separation vectors before and after the alternation should correspond to the same MU, in order to track the activity of a specific MU continuously. In the current study, the MUAP similarity index was used to determine whether two separation vectors obtained from different EMG data segments represented the same MU. The MUAP similarity index was effective to ensure consistency of the MU before and after separation vector update, because the accuracy would decrease dramatically if the updated separation vector was assigned to a different MU. The selection of the threshold value for the MUAP similarity index was largely based on our preliminary testing. Decreasing the threshold could increase the possibility of the separation vectors being updated, which can potentially further improve the accuracy. However, during experiment, the MUAP templates may not be accurately estimated due to a lack of firing events, or two distinct MUs may show similar shapes. Therefore, an adaptive adjustment procedure might be needed to identify the optimal threshold. Other measures may also be needed to determine whether two separation vectors belong to the same MU.

Updating the separation vector of MUs was a random process. During each matrix update, not all the MUs can obtain a new separation vector. This could partly explain the results that the accuracy improvement averaged across MUs (Fig. 6 and 7) was smaller compared with the representative MUs shown in Fig. 5. However, a statistically significant improvement in decomposition accuracy was observed with updated separation matrix, compared with the method without update. In addition, the results showed that the MU rotation level had a significant influence on the degree of accuracy improvement, in that more frequent rotation could reduce the performance improvement from the matrix update procedures. This indicates that the matrix updating interval needs to be shortened when the rotation occurred more frequently. In Figs. 5C and 5D, the matrix update method showed its ability to obtain an accurate separation vector for a specific MU when the

initial separation vector was inaccurate, which demonstrated a self-correcting capability for the separation matrix of the adaptive decomposition method. This is important for real-time neural decoding of sustained muscle contractions, during which the overall decomposition accuracy is maintained at a reasonable level to ensure accurate motor intent detection.

We also observed that the decomposition accuracy near the end (25-30 min) of the trial was similar regardless of whether the separation matrix was updated or not. As shown in Fig. 3A, the level of neural drive near the end (25-30 min) was similar to that of the initialization phase (first 25 seconds). As a result, the MU recruitment between these two periods were similar, and the separation matrix obtained from the initialization phase could extract spikes near the end of the trial at a similar accuracy level compared with that of the initialization phase. In contrast, the performance difference was larger during the middle (10-25 min) of the trial, mainly because the level of neural drive was higher compared to the initial period. At a higher level of neural drive, more MUs were recruited, resulting in a degraded decomposition performance without the matrix update. The results demonstrated the effectiveness of the matrix update method on maintaining the decomposition performance despite of MU recruitment-decruitment patterns, especially when new MUs were recruited.

One limitation of the current study was that our separation matrix update method was only tested on simulated EMG signals. The main advantage of simulated data is that the ground-truth of the MU activities are known, which allowed us to investigate the performance (identifiable MU number and spike detection accuracy) of our method. In future studies, we plan to evaluate our adaptive decomposition method using experimental EMG recordings. Because the ground-truth of MU activities is not available, the evaluation of the real-time force estimation performance with and without matrix update can be used to investigate the effectiveness of our method. Another limitation was that our MU simulation did not include firing rate decline over sustained activation due to fatigue or potentiation, which was observed frequently in experiments. However, we expect that our adaptive algorithm can still capture the reduced firing rate of active MUs, given that firing rate variation is often accompanied by MUAP amplitude variations, and our matrix update procedures demonstrated robust decomposition performance in this scenario.

In addition, certain algorithm parameters, such as the minimum number of spikes needed to extract the MUAP, the MUAP similarity index threshold, and the threshold of spike synchronization level, were selected mainly based on the preliminary test. The optimal selection of these parameters should be investigated in future studies. The parameter selection depends on the degree of the MUAP amplitude drift and the frequency of MU rotation. For example, a higher rate of amplitude drift and a more frequent MU rotation possibly need a smaller update interval.

During prolonged muscle contractions, besides MUAP amplitude drift, other non-stationarities can also occur, such as MUAP shape variations. In the study, only MUAP amplitude drift was considered mainly because the drift of the MUAP amplitude was believed to be one major factor that affects the decomposition performance. Our results demonstrated that the matrix update

algorithm can improve the decomposition performance regardless of the level of amplitude drift. Even though the MUAP shape was not varied in the current study, we would expect that the algorithm is not sensitive to MUAP shape variation, because the update of the separation matrix periodically re-calculate the separation vectors corresponding to the local optimal solution. However, more realistic biophysical-based EMG models [35], [36] are needed to simulate variations of MUAP shape, in order to assess the algorithm performance more comprehensively.

## V. CONCLUSION

We developed an adaptive real-time MU decomposition method based on a parallel-double-thread calculation, in order to accommodate sporadic MU recruitment-derecruitment patterns and MUAP amplitude drift over sustained muscle activations. By updating the separation matrix periodically, our method was capable of identifying a large number of MUs and improving the accuracy of the identified MUs despite of MU rotation and MUAP amplitude drift during long-term muscle contractions. Further development of our method can potentially improve the performance of the neural-machine interface systems that utilize MU discharge information to control assistive or rehabilitative devices. In addition, the MU rotation model developed in our study can be used to mimic sporadic recruitment and de-recruitment patterns of MUs, which can be integrated into the original MU pool model for the simulation of long-term MU activation.

#### REFERENCES

- [1] E. G. T. Liddell and C. S. Sherrington, "Recruitment and some other features of reflex inhibition," *Proc. R. Soc. London. Ser. B. Biol. Sci.*, vol. 97, no. 686, pp. 488–518, 1925.
- [2] C. De Luca *et al.*, "Behaviour of human motor units in different muscles during linearly varying contractions," *J. Physiol.*, vol. 329, no. 1, pp. 113–128, 1982.
- [3] F. E. Zajac and J. S. Faden, "Relationship among recruitment order, axonal conduction velocity, and muscle-unit properties of type-identified motor units in cat plantaris muscle," *J. Neurophysiol.*, vol. 53, no. 5, pp. 1303–1322, 1985.
- [4] W. Yao, R. J. Fuglevand, and R. M. Enoka, "Motor-unit synchronization increases EMG amplitude and decreases force steadiness of simulated contractions," *J. Neurophysiol.*, vol. 83, no. 1, pp. 441–452, 2000.
- [5] T. I. Sun, J. I. Chen, and T. H. Lin, "Analysis of motor unit firing patterns in patients with central or peripheral lesions using singular-value decomposition," *Muscle Nerve*, vol. 23, no. 7, pp. 1057–1068, 2000.
- [6] K. SøGaard, "Motor unit recruitment pattern during low-level static and dynamic contractions," *Muscle Nerve*, vol. 18, no. 3, pp. 292–300, 1995.
- [7] D. Farina et al., "Man/machine interface based on the discharge timings of spinal motor neurons after targeted muscle reinnervation," *Nature Biomed. Eng.*, vol. 1, no. 2, 2017, Art. no. 0025.
- [8] M. D. Twardowski et al., "Motor unit drive: A neural interface for realtime upper limb prosthetic control," J. Neural Eng., vol. 16, no. 1, 2018, Art. no. 016012.
- [9] C. Dai, Y. Cao, and X. Hu, "Prediction of individual finger forces based on decoded motoneuron activities," *Ann. Biomed. Eng.*, vol. 47, no. 6, pp. 1357–1368, 2019.
- [10] C. Dai, Y. Zheng, and X. Hu, "Estimation of muscle force based on neural drive in a hemispheric stroke survivor," *Front. Neurol.*, vol. 9, 2018, Art no 187
- [11] C. Dai and X. Hu, "Finger joint angle estimation based on motoneuron discharge activities," *IEEE J. Biomed. Health Inform.*, vol. 24, no. 3, pp. 760–767, Mar. 2020.
- [12] T. Kapelner et al., "Predicting wrist kinematics from motor unit discharge timings for the control of active prostheses," J. Neuroeng. Rehabil., vol. 16, no. 1, 2019, Art. no. 47.
- [13] E. D. Adrian and D. W. Bronk, "The discharge of impulses in motor nerve fibres: Part I. Impulses in single fibres of the phrenic nerve," *J. Physiol.*, vol. 66, no. 1, pp. 81–101, 1928.

- [14] R. S. Lefever, A. P. Xenakis, and C. J. De Luca, "A procedure for decomposing the myoelectric signal into its constituent action potentials—Part II: Execution and test for accuracy," *IEEE Trans. Biomed. Eng.*, vol. BME-29, no. 3, pp. 158–164, Mar. 1982.
- [15] R. S. LeFever and C. J. De Luca, "A procedure for decomposing the myoelectric signal into its constituent action potentials—Part I: Technique, theory, and implementation," *IEEE Trans. Biomed. Eng.*, vol. BME-29, no. 3, pp. 149–157, Mar. 1982.
- [16] C. J. De Luca et al., "Decomposition of surface EMG signals," J. Neurophysiol., vol. 96, no. 3, pp. 1646–1657, 2006.
- [17] A. Holobar and D. Zazula, "Multichannel blind source separation using convolution kernel compensation," *IEEE Trans. Signal Process.*, vol. 55, no. 9, pp. 4487–4496, Sep. 2007.
- [18] H. Nakamura et al., "The application of independent component analysis to the multi-channel surface electromyographic signals for separation of motor unit action potential trains: Part I—Measuring techniques," J. Electromyogr. Kinesiol., vol. 14, no. 4, pp. 423–432, 2004.
- [19] H. Nakamura et al., "The application of independent component analysis to the multi-channel surface electromyographic signals for separation of motor unit action potential trains: Part II—Modelling interpretation," J. Electromyogr. Kinesiol., vol. 14, no. 4, pp. 433–441, 2004.
- [20] C. Dai and X. Hu, "Independent component analysis based algorithms for high-density electromyogram decomposition: Systematic evaluation through simulation," *Comput. Biol. Med.*, vol. 109, pp. 171–181, 2019.
- [21] C. Dai and X. Hu, "Independent component analysis based algorithms for high-density electromyogram decomposition: Experimental evaluation of upper extremity muscles," *Comput. Biol. Med.*, vol. 108, pp. 42–48, 2019
- [22] M. Chen and P. Zhou, "A novel framework based on FastICA for high density surface EMG decomposition," *IEEE Trans. Neural Syst. Rehabil.* Eng., vol. 24, no. 1, pp. 117–127, Jan. 2016.
- [23] F. Negro et al., "Multi-channel intramuscular and surface EMG decomposition by convolutive blind source separation," J. Neural Eng., vol. 13, no. 2, 2016, Art. no. 026027.
- [24] V. Glaser, A. Holobar, and D. Zazula, "Real-time motor unit identification from high-density surface EMG," *IEEE Trans. Neural Syst. Rehabil. Eng.*, vol. 21, no. 6, pp. 949–958, Nov. 2013.
- [25] Y. Zheng and X. Hu, "Real-time isometric finger extension force estimation based on motor unit discharge information," *J. Neural Eng.*, vol. 16, no. 6, 2019, Art. no. 066006.
- [26] P. Bawa and C. Murnaghan, "Motor unit rotation in a variety of human muscles," J. Neurophysiol., vol. 102, no. 4, pp. 2265–2272, 2009.
- [27] P. Bawa et al., "Rotation of motoneurons during prolonged isometric contractions in humans," J. Neurophysiol., vol. 96, no. 3, pp. 1135–1140, Sep. 2006.
- [28] M. A. Pascoe et al., "Discharge characteristics of motor units during long-duration contractions," Exp. Physiol., vol. 99, no. 10, pp. 1387–1398, Oct. 2014.
- [29] A. J. Fuglevand, D. A. Winter, and A. E. Patla, "Models of recruitment and rate coding organization in motor-unit pools," *J. Neurophysiol.*, vol. 70, no. 6, pp. 2470–2488, 1993.
- [30] Y. Zheng and X. Hu, "Interference removal from electromyography based on independent component analysis," *IEEE Trans. Neural Syst. Rehabil. Eng.*, vol. 27, no. 5, pp. 887–894, May 2019.
- [31] X. Hu, W. Z. Rymer, and N. L. Suresh, "Motor unit pool organization examined via spike-triggered averaging of the surface electromyogram," *J. Neurophysiol.*, vol. 110, no. 5, pp. 1205–1220, 2012.
- [32] D. Arthur and S. Vassilvitskii, "K-Means++: The advantages of careful seeding,", in *SODA '07: Proc. 18th Annual ACM-SIAM Symp. Discrete Algorithms*, New Orleans, LA, USA, Jan. 2007, pp. 1027–1035.
- [33] Y. Zheng and X. Hu, "Concurrent prediction of finger forces based on source separation and classification of neuron discharge information," *Int. J. Neural Syst.*, vol. 31, no. 6, 2021, Art. no. 2150010.
- [34] Y. Zheng and X. Hu, "Concurrent estimation of finger flexion and extension forces using motoneuron discharge information," *IEEE Trans. Biomed. Eng.*, vol. 68, no. 5, pp. 1638–1645, May 2021.
- [35] J. Duchene and J. Y. Hogrel, "A model of EMG generation," *IEEE Trans. Biomed. Eng.*, vol. 47, no. 2, pp. 192–201, Feb. 2000.
- [36] D. Farina et al., "A surface EMG generation model with multilayer cylindrical description of the volume conductor," *IEEE Trans. Biomed. Eng.*, vol. 51, no. 3, pp. 415–426, Mar. 2004.